V

Publication V

Majander P., Siikonen T., Large-eddy simulation of a round jet in a cross-flow, International Journal of Heat and Fluid Flow, vol 27, pp 402-415, 2006.

Available online at www.sciencedirect.com
SCIENCE DIRECT
International Journal of Heat and Fluid Flow 27 (2006) 402–415
International Journal of HEAT AND FLUID FLOW
www.elsevier.com/locate/ijhff

Large-eddy simulation of a round jet in a cross-flow

Petri Majander *, Timo Siikonen

Helsinki University of Technology, Laboratory of Applied Thermodynamics, FIN-002015 Helsinki, Finland

Received 10 December 2004; received in revised form 4 January 2006; accepted 13 January 2006
Available online 3 March 2006

Abstract

A large-eddy simulation (LES) of a round jet penetrating normally into a cross-flow is described. The jet-to-cross-flow velocity ratio is 2.3 at a Reynolds number of 46,700, based on the jet bulk velocity and the jet diameter. The simulations are performed with steady and unsteady boundary conditions. A passive scalar is discretized either with a central or a TVD discretization. The results are compared with each other and the experimental measurements of Crabb, Durão and Whitelaw. The computation reproduced many phenomena present in such a flow, like the shear layer ring vortices and a counter-rotating vortex pair. In general, a reasonable agreement with the measurements was obtained. However, the calculation predicts an intense backflow low near the flat wall. As the measured points do not reach this area it is possible that such a recirculation exists but in any case the LES predicts it too high above the wall and probably too intense. The unsteady boundary condition increases the spreading of the jet slightly.

Keywords: Large-eddy simulation; Jet in cross-flow; Passive scalar

1. Introduction

Jets in a cross-flow are complex flows with many practical applications ranging from jets into combustors to V/STOL aircraft in transition flight. Perhaps the most familiar example in everyday life would be smoke rising from a chimney into a crosswind. Due to the great practical relevance, many experimental, numerical and theoretical studies have been undertaken. Here only a few are cited. Keffer and Baines (1963) measured the trajectory of the jet and the velocity along it. The turbulent intensity was also measured along a line in the plane orthogonal to the jet trajectory. A more complete survey was conducted by Crabb et al. (1981) who measured mean and fluctuating velocity magnitudes with a laser-Doppler anemometer near the jet exit and hot wires further downstream. This flow is the subject of a simulation in the present research. Andreopoulos and Rodi (1984) used a triple wire probe to simultaneously measure all three components of velocity. Kelso et al. (1996) studied the structure of round jets in cross-flows using flow visualization techniques and flying-hot-wire measurements. The jet-to-cross-flow velocity ratios ranged from 2 to 4 and the Reynolds numbers varied between 440 and 6200, based on the jet diameter and free-stream velocity.

Jets in a cross-flow have also been studied numerically and here two examples are paid attention to. Yuan et al. (1999) performed large-eddy simulations (LES) at two jet-to-cross-flow velocity ratios, 2.0 and 3.3, and two Reynolds numbers, 1050 and 2100, based on the cross-flow velocity and the jet diameter. They discretized the computational area into a total of 1.34×10^6 control volumes. The jet in a cross-flow measured by Crabb et al. (1981) was modelled with LES by Wille (1997). He used both a coarse and a fine mesh, which included 88,440 and 997,920 mesh points, respectively. Considering the Reynolds number of 46,700, based on the jet bulk velocity and the jet exit diameter, both grids are quite coarse even if the near-wall boundary layers were modelled. Wille (1997) does not explicitly state whether the Reynolds number is the same

* Corresponding author.
E-mail addresses: Petri.Majander@tkk.fi, Petri.Majander@hut.fi (P. Majander).

0142-727X/$ - see front matter © 2006 Elsevier Inc. All rights reserved.
doi:10.1016/j.ijheatfluidflow.2006.01.004

as in the experiment. Wegner et al. (2004) studied turbulent mixing using LES. They varied the angle between the jet and the cross-flow. The mixing was enhanced as the angle was increased i.e. as the jet was directed against the cross-flow. The baseline flow in their simulation was that measured by Andreopoulos and Rodi (1984).

In this study a parallel solver developed at the laboratory of the Applied Thermodynamics in Helsinki University of Technology is used to compute an LES of a jet in a cross-flow measured by Crabb et al. (1981) and a comparison to the experiment is carried out. In the next chapter, the governing equations and the numerical methods are presented. In Section 3, the characteristics of the computational case are described. The results are shown and compared to the measurements in Section 4, and finally in Section, the conclusions are drawn.

2. Governing equations

The filtered LES equations for isothermal incompressible flows with a passive scalar θ transport are written as

$$\frac{\partial \bar{u}_i}{\partial x_i} = 0, \tag{1}$$

$$\frac{\partial \bar{u}_i}{\partial t} + \frac{\partial \bar{u}_i \bar{u}_j}{\partial x_j} = -\frac{1}{\rho}\frac{\partial \bar{p}}{\partial x_i} + \frac{\partial}{\partial x_j}(\nu 2\overline{S}_{ij} - \tau_{ij}), \tag{2}$$

$$\frac{\partial \bar{\theta}}{\partial t} + \frac{\partial \bar{\theta}\bar{u}_j}{\partial x_j} = \frac{\partial}{\partial x_j}\left(\alpha\frac{\partial \bar{\theta}}{\partial x_j} - q_j\right), \tag{3}$$

where $\bar{u}_i$ are velocity components, $\bar{p}$ is pressure and ρ is a constant density. Molecular viscosity and diffusivity are denoted by ν and α. The strain rate tensor is

$$\overline{S}_{ij} = \frac{1}{2}\left(\frac{\partial \bar{u}_i}{\partial x_j} + \frac{\partial \bar{u}_j}{\partial x_i}\right). \tag{4}$$

The sub-grid scale stress and scalar flux are

$$\tau_{ij} = \overline{u_i u_j} - \bar{u}_i \bar{u}_j, \tag{5}$$

$$q_j = \overline{\theta u_j} - \bar{\theta}\bar{u}_j, \tag{6}$$

respectively. The Boussinesq approximation

$$\tau_{ij} - \frac{\delta_{ij}}{3}\tau_{kk} = -2\nu_{\mathrm{sgs}}\overline{S}_{ij} \tag{7}$$

relates sub-grid scale stresses τ_{ij} to the eddy viscosity ν_{sgs} and the resolved-scale strain rate tensor $\overline{S}_{ij}$. Smagorinsky (1963) introduced the eddy viscosity model written as

$$\nu_{\mathrm{sgs}} = (C_s \Delta)^2 |\overline{S}|, \tag{8}$$

where C_s is called a Smagorinsky constant, Δ is a length scale defined here as $V^{1/3}$ and $|\overline{S}| = \sqrt{2\overline{S}_{ij}\overline{S}_{ij}}$. The length scale represents the cell size and it is usually computed as $V^{1/3}$. A value of 0.17 for C_s was used in this work with no damping near the wall. The sub-grid scale scalar flux is modelled analogously with a mixing length gradient model

$$q_j = -\frac{\nu_{\mathrm{sgs}}}{Pr_{\mathrm{sgs}}}\frac{\partial \bar{\theta}}{\partial x_j}. \tag{9}$$

Depending on the flow, molecular Prandtl number Pr and the direction and the distance of the scalar flux to the wall, Cabot and Moin (1993) have presented values for the turbulent Prandtl number Pr_{sgs} ranging from 0.3 to 0.8. Here a constant value of 0.6 is used.

3. Flow solver

The simulation is performed with a parallel SIMPLE-based Navier–Stokes solver developed at Laboratory of Applied Thermodynamics, Helsinki University of Technology. A body-fitted co-ordinate system is implemented with a co-located and structured finite-volume technique. Multi-block meshes are used to solve flows in complex domains. The parallelization takes advantage of the multi-block decomposition, each block is assigned to its own processor. The boundary values between the processes are exchanged with message passing library (MPI). For large-eddy simulation a second-order central difference is used for a spatial discretization and a second-order three-level implicit method for time stepping. Within a time step the solution is iterated. The Poisson equations for the momenta, pressure and scalars are solved in a series with an algebraic multi-grid solver. Details of the method and validation benchmarks are available by Majander and Siikonen (2003a,b).

4. Flow configuration

The setup of the jet in a cross-flow is sketched in Fig. 1. The Reynolds number $Re_D = 46{,}700$ referred to the pipe flow is rather large for an LES of the whole jet. Therefore the computational domain has been reduced from that of the wind tunnel used by Crabb et al. (1981). The domain

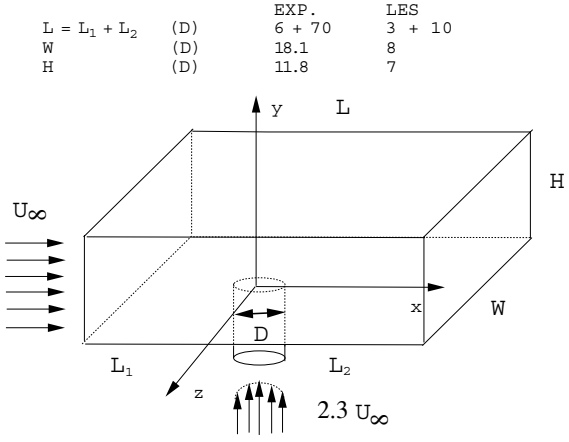

Fig. 1. Schematics of the domain in the jet in a cross-flow. The experiment refers to the wind tunnel used by Crabb et al. (1981) whereas the LES refers to the present computational domain size.

size used by Wille (1997) is $12D \times 6D \times 6D$ and it was suspected that the domain restricted the spreading of the jet, therefore the present domain is slightly larger. The number of the control volumes (CVs) is $192 \times 96 \times 144$ in stream-wise, wall-normal and span-wise direction, respectively. In addition to this, a jet pipe is represented with 110,592 CVs, altogether 2,764,800 CVs, which are equally distributed into 25 blocks. The grid is clustered around the jet exit and the height of the first cell from the lower wall is $0.002D$, which corresponds to $\Delta y^+ = 4.7$ if scaled by the friction velocity of the incoming turbulent pipe flow. The stretching factor in the wall-normal direction is less than 1.06. Crabb et al. (1981) used laser-Doppler anemometry near the jet from $x/D = -1$ to 6. The uncertainty of the measured mean velocity is of order 3% and that of the rms value 7%. The downstream region is measured with hot wires and the uncertainties are given as U/U_∞: ±2%, $u/U, v/U, w/U$: ±7% and $uv/U, uw/U, vw/U$: ±15%. Crabb et al. (1981) found that without the jet, the height of the boundary layer in front of the jet exit was about $0.24D$ high and the free-stream turbulence level of the channel is 0.6%. Two different boundary conditions are applied. First a uniform cross-velocity U_∞ was set at the inlet.

An unsteady condition was extracted from a turbulent profile from half the channel flow $0.22D$ high. Above this boundary layer a non-shear turbulent flow was set so that the fluctuations were gradually damped to zero by $y/D = 0.5$. Above that a constant value was used preserving the same mass flow through the inlet as the steady-state boundary condition.

At the lateral and top surfaces free-slip boundary conditions are applied and a no-slip condition is forced at the bottom wall. At the outlet a zero-gradient (Neumann) condition (NBC) is used. Majander (2000) has compared the CBC with the NBC in a shedding cylinder flow. The CBC excelled over NBC only if the outlet boundary was located very close to the cylinder. Wille (1997) used the CBC, but he found that there was virtually no effect on

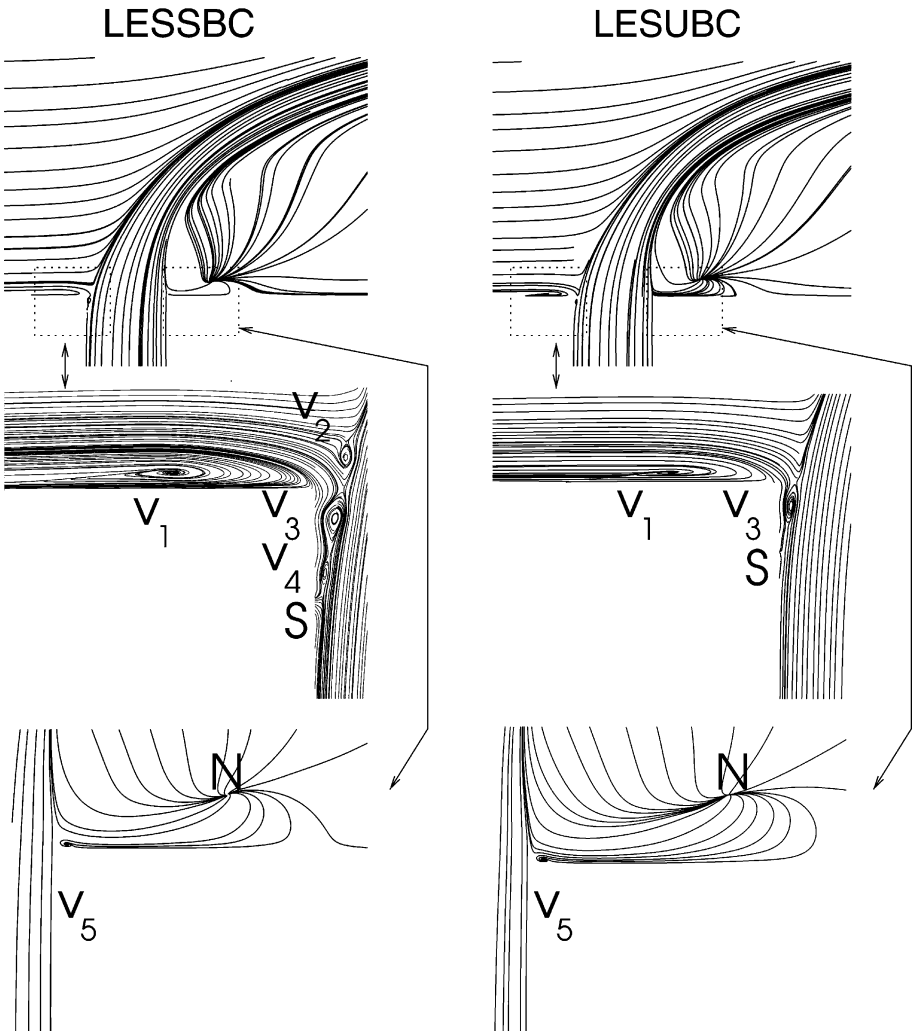

Fig. 2. The streamlines of the mean velocities in the symmetry plane with different boundary conditions. In the second row magnifications upstream from the jet exit. The separation zone is smaller inside the pipe with LESUBC including only one vortex V_3. The lee of the jet (bottom) shows a node (N) and a vortex (V_5).

the predicted first and second moments, as the two conditions were tested with the plane jet in a cross-flow.

Andreopoulos (1982) has studied experimentally the flow field near the outlet of the jet pipe. He found that at $-D/2$ the pipe flow profile is only slightly skewed as the jet-to-cross-flow velocity ratio is 2. By measuring the wall static pressures he defines the upstream effect to be about $1.6D$. In current computation the inlet pipe is $1D$ long, which is thought to be far enough to catch the essential upstream effects.

First the case was calculated with a steady fully developed turbulent profile. The unsteady condition was obtained from an LES of a fully developed pipe flow. The topology of the mesh and the time-step size were different in the precursor computation. Therefore the boundary condition velocities were interpolated spatially and temporally in the jet computation. The sequence of the boundary values was also interpolated to be periodic, whose duration corresponds to the bulk flow advancement of two diameters in the inlet pipe.

Wille (1997) defined the vertical velocity profile at the jet exit from the dynamic pressure and the tangential velocities were zero at the lower wall, which prevents the interaction between the incoming pipe flow and the cross-flow. A zero-gradient pressure surrounds the whole area and the average pressure level in the area is fixed. Crabb et al. seeded the jet with helium trace and measured the mixture fraction θ/θ_J at different locations downstream. In the cross-flow inlet $\theta/\theta_J = 0$ and in the jet $\theta/\theta_J = 1$. A zero-gradient for the scalar is set at all the other boundaries. Turbulent Prandtl or Schmidt number was set to a constant value of 0.6.

The startup of the calculation was quite difficult. The dynamic model did not stabilize the computation and consequently it was not used. An excessive value for the Smagorinsky constant C_s was set, until after some transient time, it was lowered to a value of 0.17. Also, an underrelaxation of a few percent was added to the diagonal of the pressure correction equation in order for the MG solver to converge. The time step was rather short, $\Delta t = 0.005T$, where $T = D/2U_b$. This implies that the bulk cross-flow advances from the inlet to the outlet during 5200 time steps. Due to the relatively thin cells the highest CFL-values are around 4 at the jet exit, however. A total of 15 sub-iterations was calculated during a time step. It might have been possible to obtain the same results with a smaller amount of iterations, but this was not tested. The global mass balance residual reduced to a third from the first iteration, which is a rather poor convergence within a time step. Since the time step is globally so small, a global mass error remains small even at the first iteration cycle. The flow was computed a time of $113T$ from the initial state before statistics were gathered. The statistics were gathered

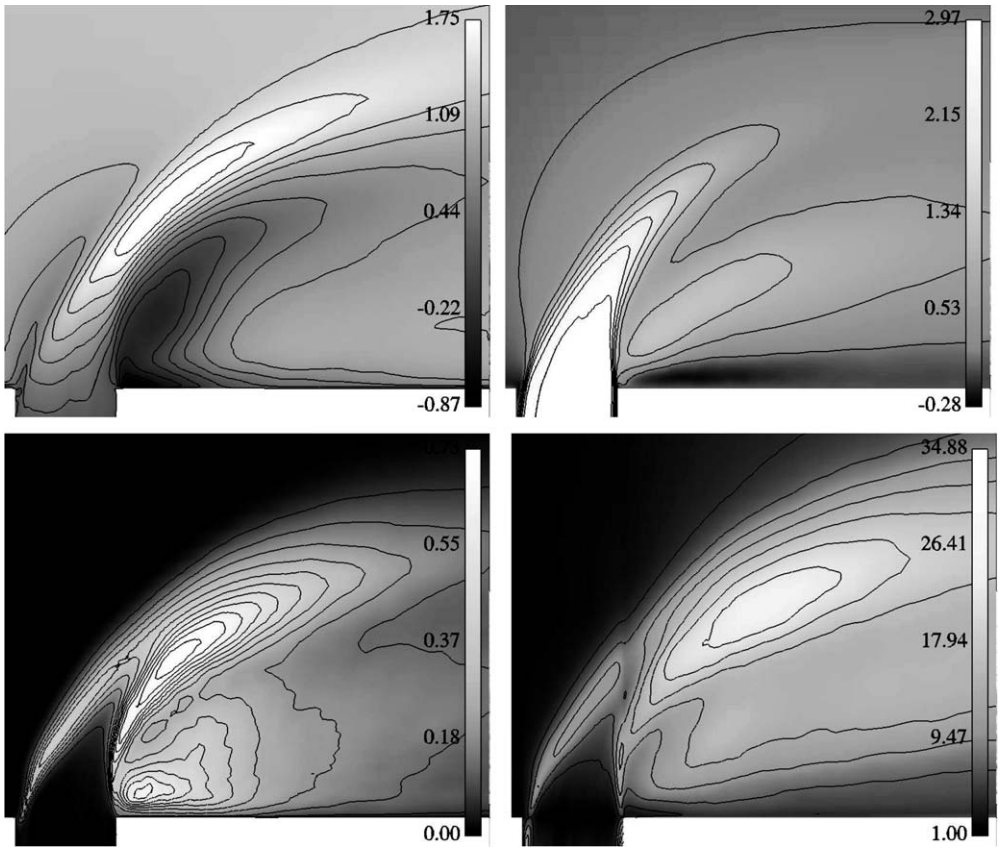

Fig. 3. At the top row: Mean stream-wise velocity U/U_∞ (left) and vertical velocity V/U_∞ contours (right) in the symmetry plane. At the bottom row: Turbulent kinetic energy $\frac{\overline{u'_i u'_i}}{2U_\infty^2}$ and eddy viscosity $\frac{\overline{\nu+\nu_{sgs}}}{\nu}$ contours in the symmetry plane.

during $153T$, or six flow-through times. The results were relatively converged after $87T$, especially near the jet exit. The biggest changes were seen in non-diagonal stresses in the far field at $x/D = 8$. There was no need to reconsider the conclusions due to the continued computation, however. In calendar time all this corresponds to approximately 40 days when using 25 Power4 processors of an IBM SP cluster. With the unsteady boundary condition the statistics were gathered a time of 7.5 flow-through times.

5. Results

5.1. Flow field

In this section a qualitative overview on the flow field is given. The mean flow streamlines in the jet exit region are shown in Fig. 2. There are some differences between the solutions with the steady and the unsteady BC at the inlet pipe, which from now on are referred to as LESSBC and LESUBC, respectively. Both cases are referred to as LES in general. In the central plane upstream of the jet exit there is a single vortex (V_1), whose centre is located $0.25D$ upstream of the lip. Kelso et al. found that at a smaller Reynolds number $U_\infty D/v = 1600$ there were two vortices in front of the jet, separated by a saddle point. They also visualized a 'hovering vortex' above the jet exit. The vortex originates from the collision of the jet and the cross-flow shear layers. In Fig. 2 the streamlines of the LESSBC reveal three distinguishable roll-up vortices (V_2, V_3, V_4),

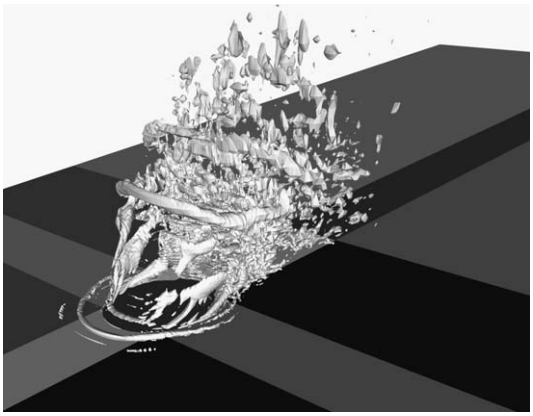

Fig. 4. An instantaneous iso-surface of the second invariant of the velocity gradient $Q = 30$.

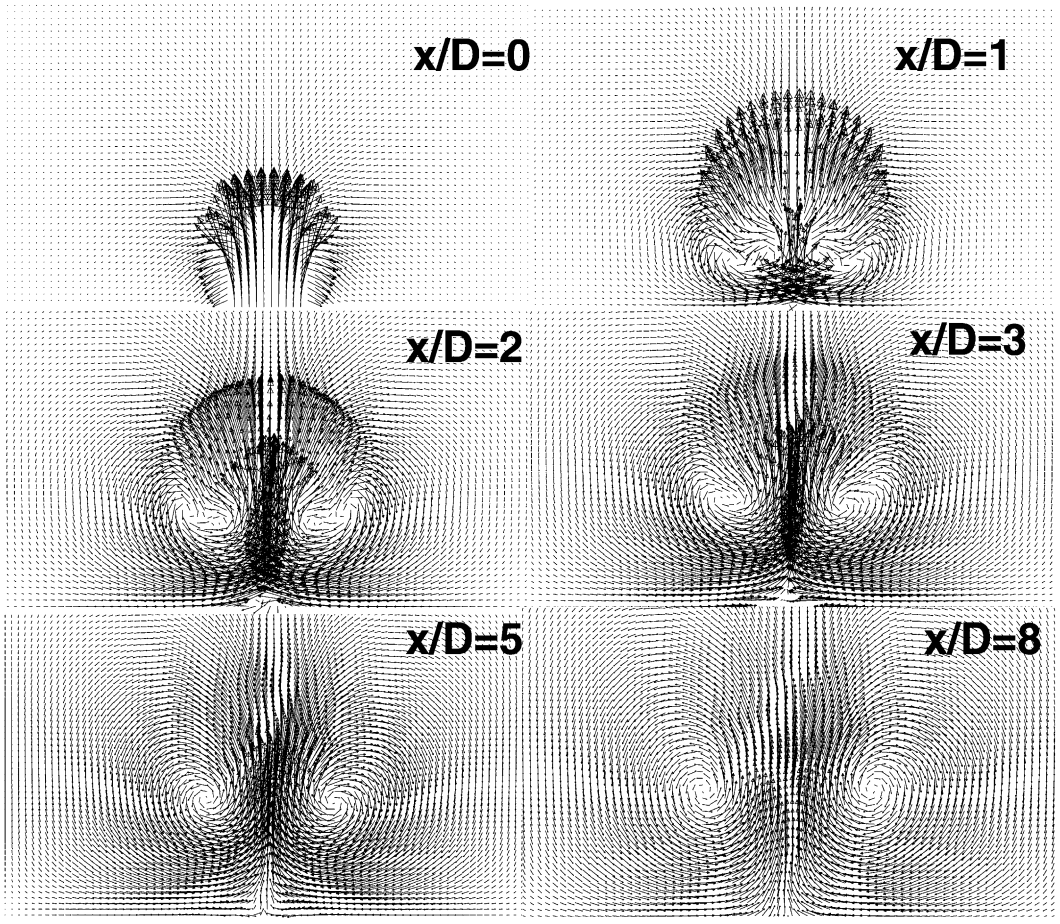

Fig. 5. Evolution of the counter-rotating vortex pair at stream-wise planes at various distances from the jet exit.

two of them inside the pipe (V_3, V_4). In LESUBC the roll-up vortex V_2 is not present and V_4 is hardly distinguishable. In both schemes some part of the cross-flow near the surface is swept into the pipe. The saddle point S, or the lowest point where the incoming fluid penetrates, is located at approximately $y/D = -0.2$. The LESUBC shows a smaller separation bubble inside the inlet pipe. At a Reynolds number 10 times smaller, and at the jet-to-cross-flow velocity ratios $R = 2.2$ and 4.0, Kelso et al. (1996) reported the saddle point locations of $y/D = -0.4$ and -0.16, respectively. At high velocity ratios ($\geqslant 6$) the saddle point is located at the lip. In the symmetry plane downstream of the jet, there resides a node (N). LESUBC predicts the location of the node slightly higher ($x/D = 1.1, y/D = 0.21$) than LESSBC ($x/D = 1.06, y/D = 0.18$). A vortex is also located right downstream of the jet exit edge (V_5). Behind the jet there is a rather strong back-flow near the flat plate, confirmed by the top row of Fig. 3 which shows the contours of the mean stream-wise and vertical velocity in the central plane. The back-flow almost reaches a velocity of the free-stream value. The cross-flow deflects over the bending jet and accelerates to a value of nearly twice the free-stream value. The mean vertical velocity contours (Fig. 3) reveal two regions of strong upward motion. The upper region is generated directly by the jet. In the lower region the upward velocity is at maximum about half of the jet velocity. This motion is the fluid flowing from the node toward the jet trajectory. Yuan et al. found that at $Re_D = 2100$ there was a clear distinction between the sign of the vertical vorticity emerging from the left-hand side and the right-hand side of the pipe (Yuan et al., 1999). This notion is confirmed in this case. The vorticity seems to mix quicker in the present case, which is probably due to the higher Reynolds number. Fig. 4 reveals the vortices with the iso-surface of the second invariant of the velocity gradient Q defined as

$$Q = -\frac{1}{2}(\overline{S}_{ij}\overline{S}_{ij} - \overline{\Omega}_{ij}\overline{\Omega}_{ij}) = -\frac{1}{2}\frac{\partial \bar{u}_i}{\partial x_j}\frac{\partial \bar{u}_j}{\partial x_i}.$$

An animation shows that the vortex upstream of the jet exit is formed and it moves to the lip of the jet exit where it seems to merge with the vortices of opposite sign rising

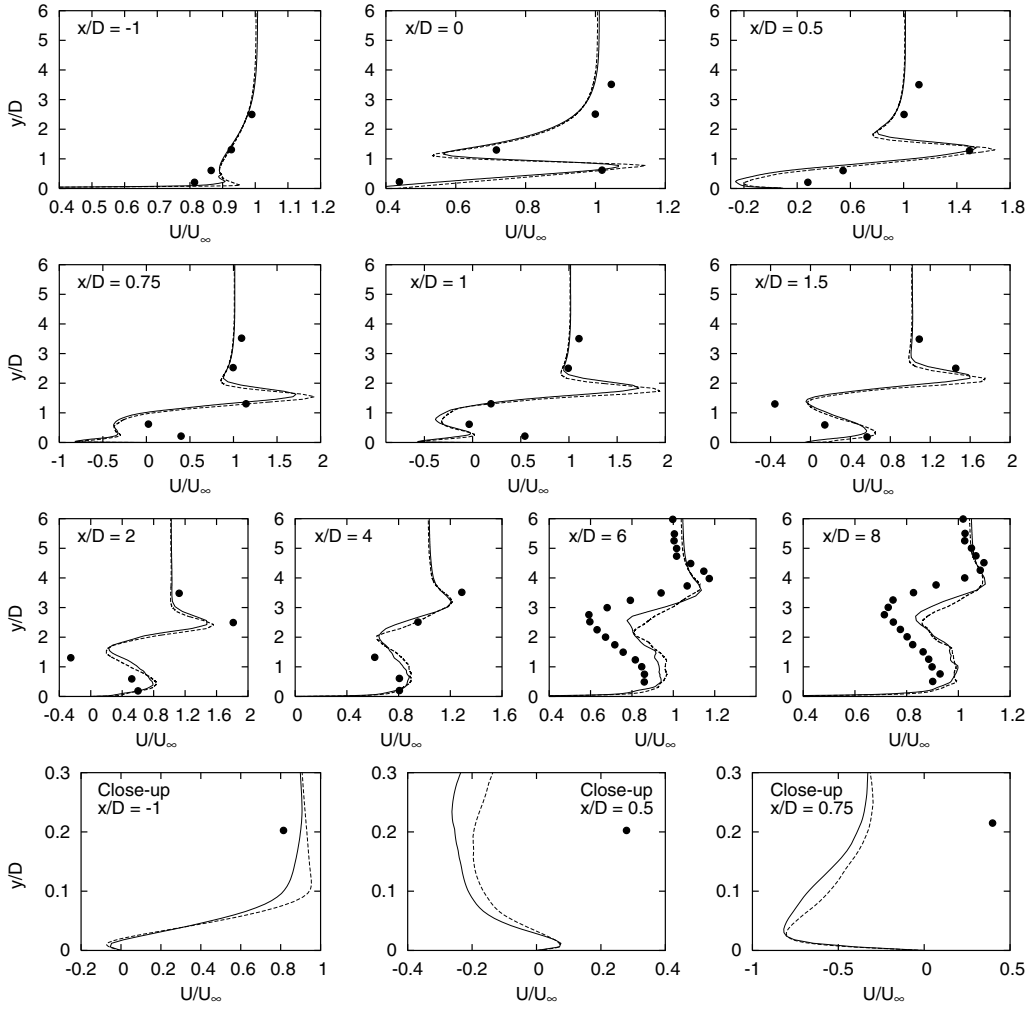

Fig. 6. Mean stream-wise velocities in the central plane, $z/D = 0$: LESUBC (—), LESSBC (---), Crabb et al. (1981) (●).

from the pipe. The merger may explain that at a distance of approximately one diameter above the exit there is weaker coherent vorticity in front of the jet.

Fig. 5 shows an evolution of a counter-rotating vortex pair (CVP) at various distances from the jet exit. A small CVP is present already at the jet exit ($x/D = 0$), which supports the idea that it is initiated by the pipe vorticity (see e.g. Kelso et al., 1996). Further downstream the CVP grows and the computational domain may constrain the spreading slightly.

The resolved turbulent kinetic energy (TKE) in the symmetry plane (Fig. 3) shows a maximum under the jet trajectory where the flow emerging from the node curves to join the jet. Another smaller maximum is located at the node behind the jet. The eddy viscosity (Fig. 3) exhibits a local maximum under the jet trajectory too, approximately in the same location as TKE. At the node there is no maximum. This is prevented by a shorter length scale due to the grid clustering or a smaller strain rate, or both. The greatest viscosity ratio, approximately 35, exists in the shear layer near the inlet of the pipe. In the inlet pipe the resolution in the boundary layer is far too coarse. As the resolved TKE is almost zero there the sub-grid scale viscosity acts more like a Reynolds-averaged model in that region. Poor accuracy is obtained inside the pipe but we assume that this is not important in the simulation of the whole jet, which is the primary focus of the present work.

5.2. Comparison to the measurements

A comparison of the calculated flow field to the experiment of Crabb et al. (1981) (CDW) is conducted next. The mean stream-wise velocities in the central plane are shown in Fig. 6. At $x/D = -1$ the present LES shows a slight acceleration near the flat wall at $y/D = 0.1$–0.2, which is due to the vortex blocking the flow. See the close-up at bottom right in Fig. 6. The turbulent boundary profile of LESUBC results in a smaller peak and CDW shows no such effect. In a real flow such a recirculation area may be closer to the wall. At the down-stream pipe wall $x/D = 0.5$ the LES predicts a small back-flow at $y/D = 0.2$ (close-up). The positive velocity over the wall $y/D = 0.02$ is connected to vortex V_5 described above. There are two minima seen in the back-flow at $x/D = 0.75$ and 1. In the LESUBC the back-flow is slightly increased. The strong back-flow near the wall nodes might be a sign of a non-physical phenomenon owing to too coarse cells for the present wall-resolved LES. On the other hand Andreopoulos and Rodi (1984) mention that in the lee of the jet with similar parameters, a reverse-flow region forms very close to the wall in which measurements were not possible. It is possible such a recirculation exists, but in any case the LES predict it too high up above the wall and probably too intense. In CDW the back-flow resides approximately between $x/D = 0.75$ and 3. In the LES there is no back-flow downstream of $x/D = 2$ and the flow profile is flatter

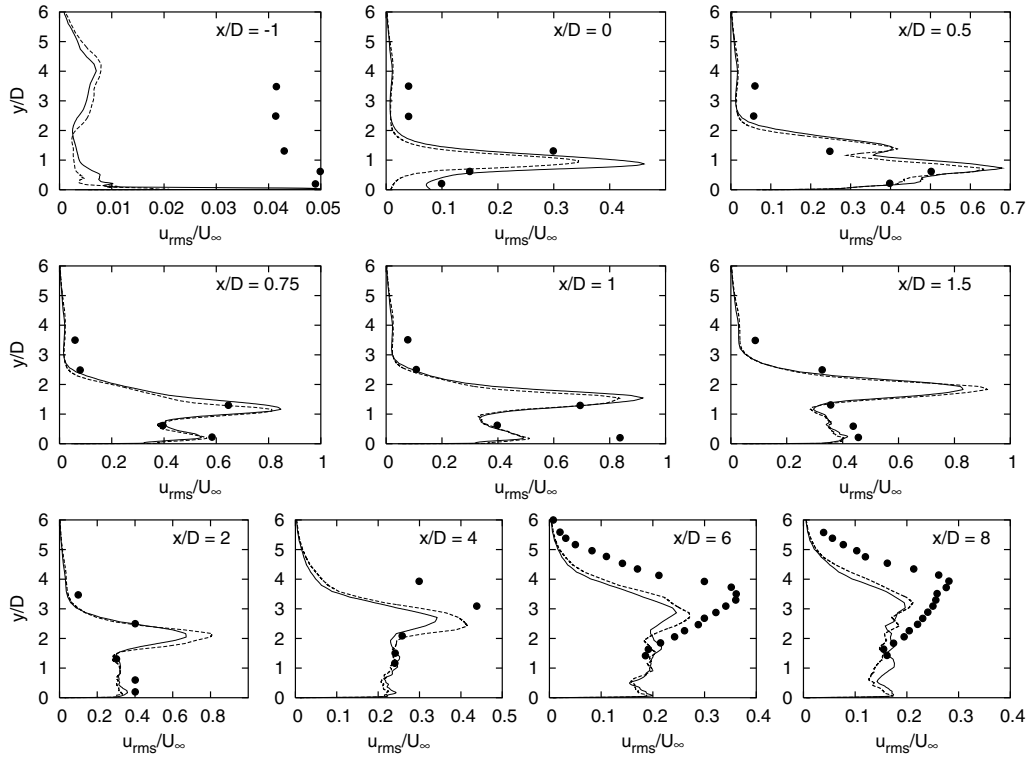

Fig. 7. Stream-wise turbulence intensities in the central plane, $z/D = 0$: LESUBC (—), LESSBC (---), Crabb et al. (1981) (●).

than that of CDW. The LESUBC shows steeper gradient in the lee of the jet $x/D > 3$.

Fig. 8 shows the stream-wise velocities plotted at various distances y/D from the wall and z/D from the central plane. This plot confirms clearly the previous conclusion. The LES predicts the intense back-flow close to the wall and to the jet exit.

The stream-wise turbulent intensity (Fig. 7) upstream of the jet is somewhat difficult to interpret. Without the jet the boundary layer width is $0.24D$ and the free-stream turbulence is less than 0.6%. It is then questionable whether the measured turbulence level of 4% originates from the upstream boundary layer at $x/D = -1$. The fluctuations above the boundary layer width originate probably from the vortex motion described above or some other interaction of the jet and cross-flow. The LES captures only part of this intensity, which may be due to the applied Smagorinsky model.

The LESUBC has a peak value $u_{\mathrm{rms}}/U_\infty = 0.05$ and LESSBC that of 0.02 near the wall at $y/D = 0.1$. Apparently, the large cells at the inlet due to the clustered mesh damped the fluctuations before interacting with the jet. The essential difference between the two cases at the cross-flow inlet is the average profile.

Downstream of the inlet there are two maxima in the intensity profile. They reside approximately at the location of the steepest gradient of the velocity. In general, the turbulent intensities are rather well predicted compared to the mean velocity.

Yuan et al. (1999) performed simulations to test the effect of different inlet conditions. They tested a plug flow profile, a mean turbulent profile and a temporally evolving

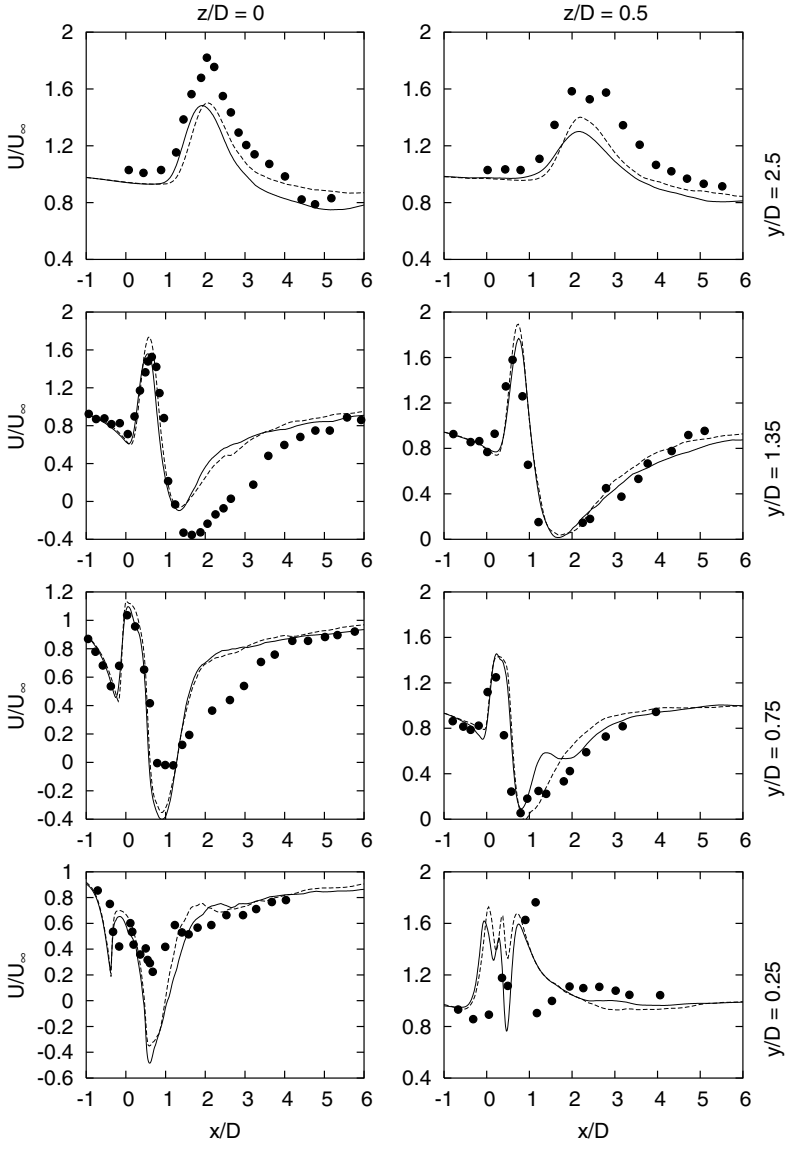

Fig. 8. Mean stream-wise velocities plotted at various distances y/D from the wall and z/D from the central plane: LESUBC (—), LESSBC (---), Crabb et al. (1981) (●).

pipe flow and reported that the latter boundary condition improved obviously the result. However, they do not provide much evidence to support this conclusion. Wille (1997) set the boundary condition at the wall by setting the lateral components to zero and the vertical component to such a value that the mean dynamic pressure was constant. Random fluctuations were added to the profile. This condition produced a surprisingly good agreement with CDW at $y/D = 0.25$ although it prevented any upstream effect from the pipe. The present jet profiles have approximately 10% higher peak values than the measured one at $y/D = 0.25$ (Fig. 9, $z/D = 0$). Crabb et al. (1981) report that the profile at the outlet is a fully developed profile in a pipe whose length was $30D$. In the present simulation there are no significant differences in the outlet profiles between LESSBC and LESUBC. The LES shows high velocity peak behind the jet indicating the intense recirculation. Half the diameter of the symmetry plane the LESUBC profiles is higher.

Further up at $y/D = 2.5$ the jet has lost momentum since both stream-wise and vertical velocities are under-predicted. The jet has probably bent more that of CDW. LESUBC shows a greater momentum deficit, especially at $z/D = 0.5$. This may indicate also an enhanced spreading.

The difference between two cases is apparent in turbulent intensities near the jet exit in Figs. 10 and 11. The wall-normal intensity in Fig. 11 shows two distinct peaks near the jet exit, corresponding to the upstream and downstream shear layers of the pipe flow. Close to the wall ($y/D = 0.25$) the LESSBC predicts a very small intensity on the upstream side, whereas both the peaks are captured by the LESUBC. In the lee of the jet the intensities are in a reasonable agreement with CDW. The back-flow generates fluctuations close to the wall also in the LESSBC,

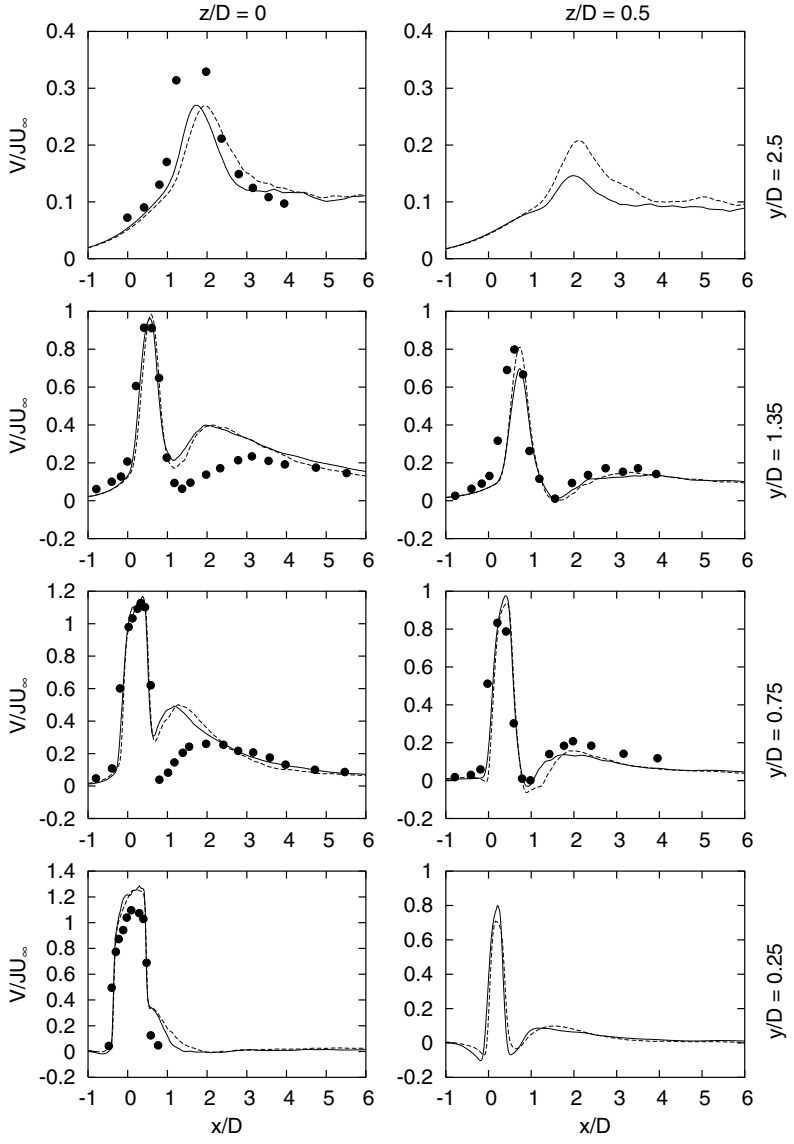

Fig. 9. Mean wall-normal velocities plotted at various distances y/D from the wall and z/D from the central plane: LESUBC (—), LESSBC (---), Crabb et al. (1981) (●).

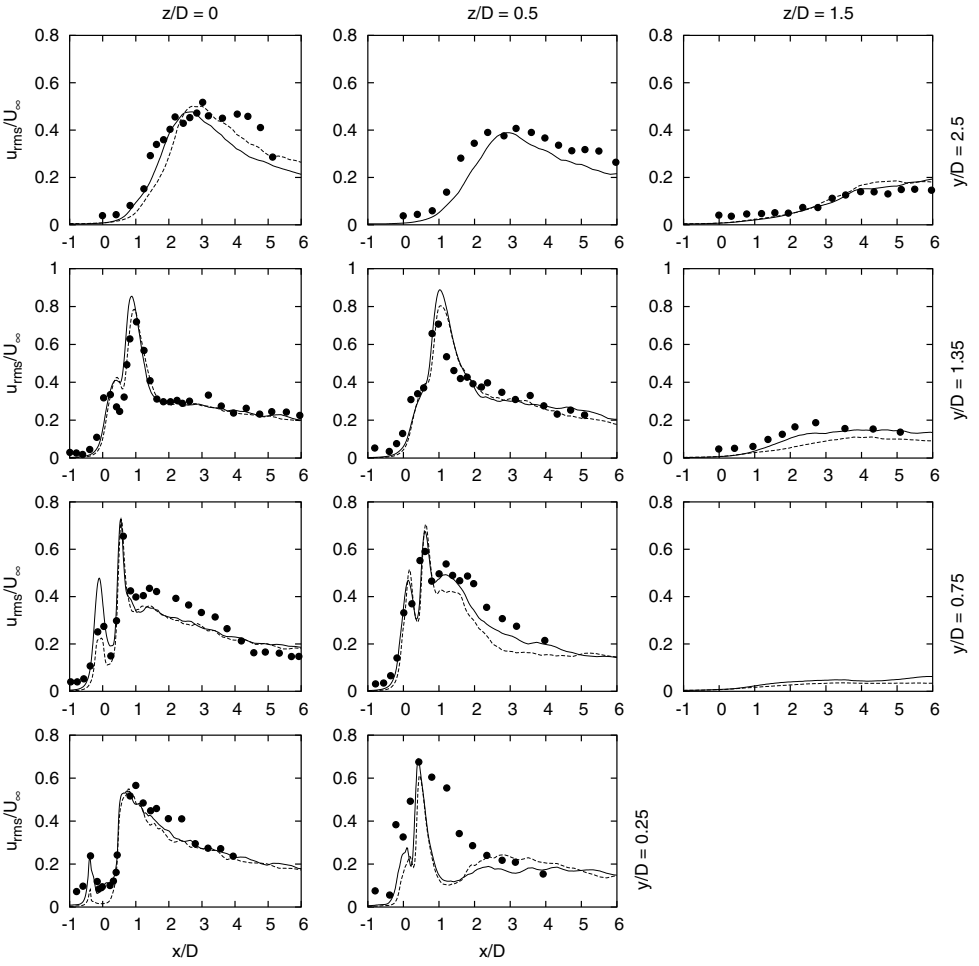

Fig. 10. Stream-wise turbulence intensities plotted at various distances y/D from the wall and z/D from the central plane: LESUBC (—), LESSBC (---), Crabb et al. (1981) (●).

and on the upstream side the fluctuations grow closer to the measured ones further up, which is probably connected to the development of the ring vortices. In Figs. 10 and 11 only resolved part of the turbulent stress is plotted. Also the total stresses including the contributions from the sub-grid scale model were gathered. Along the lines shown it is hard to distinguish the two quantities from each other as they lie within the line width. Wille (1997) observed differences in the resolved and the total stresses with a coarse grid (88,440 cells) but the differences are reported to be very small with the fine mesh (997,920 cells). In major part of the domain the modelled stresses are negligible compared to the averaged resolved ones. However, the resolved stresses consist of the large scale motion, and the modelled stress is significant in stabilizing the calculation. In the shear layers (e.g. in the inlet pipe) the modelled stresses might be large even if compared to the resolved stress. As the resolved stress is very small there, the sub-grid scale model works as a poor Reynolds-averaged model. The highest ratio ν_{sgs}/ν of approximately 35 is calculated near the pipe wall where there is little or no resolved turbulence, as shown in Fig. 3.

Fig. 12 presents lateral profiles for the plane $x/D = 8$. The simulated jet has dispersed there as the profile has become flatter than the measured one, which is seen also in Fig. 6. The Reynolds stresses are rather isotropic. In the far field velocity field the inlet pipe BC has little effect. The authors suspect that the normal stresses at $y/D = 1$ are plotted 0.1 units too high by Crabb et al. (1981) which explains most of the differences seen between the present LES and the measured results. Considering the coarse mesh in the far field and the short sampling time, the cross-stresses $\overline{u'v'}/U$ and $\overline{u'w'}/U$ are relatively well predicted. At $y/D = 1$ and 4, the measured $\overline{u'w'}/U$ is negative at the centre plane, although it should be zero, on the grounds of symmetry arguments. Either there must be an asymmetry in the flow or the measurement itself is in error.

5.3. Scalar mixing

In a preliminary calculation with a lower Reynolds number it was observed that the central difference scheme led into spurious wiggles in the scalar field. The computed mixture fraction had values lower than zero and higher than

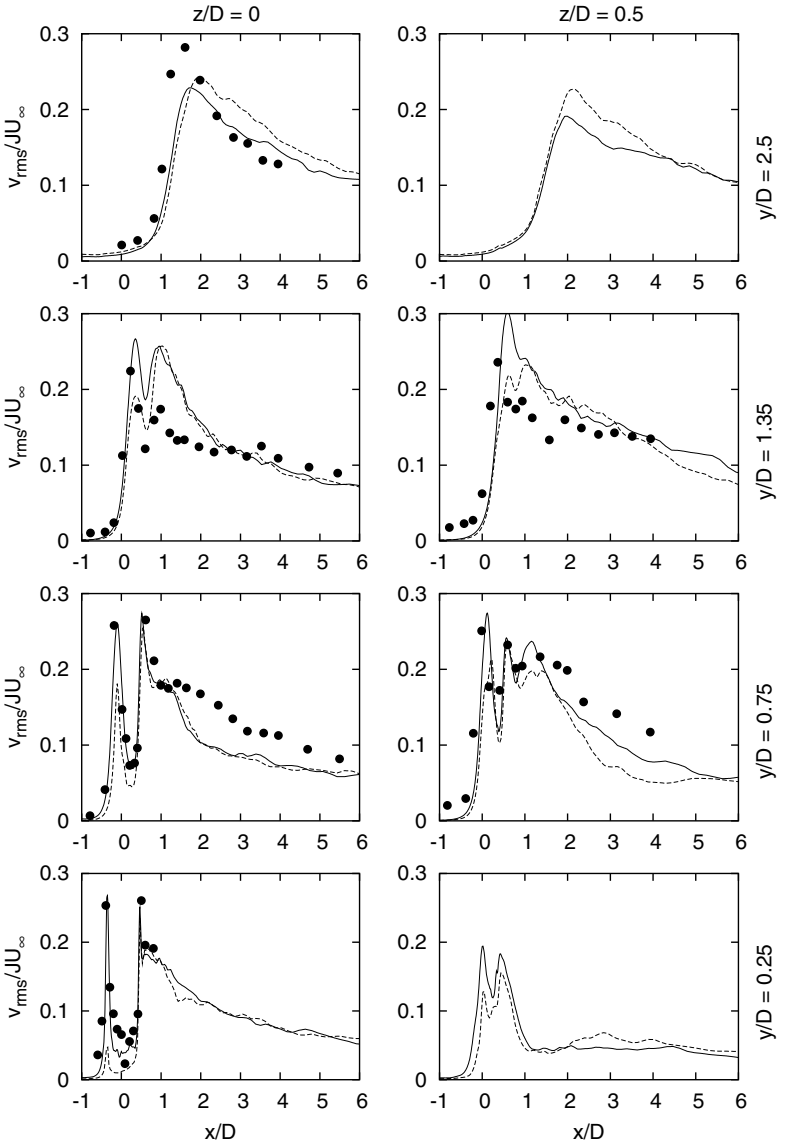

Fig. 11. Wall-normal turbulence intensities plotted at various distances y/D from the wall and z/D from the central plane: LESUBC (—), LESSBC (---), Crabb et al. (1981) (●).

one. This was observed also by Wille (1997) who thought that using a TVD scheme would be unacceptable for excessive smearing. In the mean mixing fraction the spurious values were averaged off mostly. In preliminary tests a TVD-limited central difference for scalar in the convection term reduced overshoots effectively, but not completely. Here a MUSCL scheme is used with the minmod limiter (Hirsch, 1990). With the central difference discretization the variables extrapolated at the cell face $i+\frac{1}{2}$ from left- and right-hand side are

$$\theta^{\mathrm{L}}_{i+\frac{1}{2}} = \theta_i + \frac{1}{2}\phi(r^{-}_{i+\frac{1}{2}})(\theta_{i+1} - \theta_i), \tag{10}$$

$$\theta^{\mathrm{R}}_{i+\frac{1}{2}} = \theta_{i+1} - \frac{1}{2}\phi(r^{+}_{i+\frac{1}{2}})(\theta_{i+1} - \theta_i), \tag{11}$$

where the minmod limiter is defined as

$$\phi(r) = \begin{cases} \min(r, 1), & r > 0, \\ 0, & r \leqslant 0 \end{cases}$$

and the arguments of the limiter are the ratios of the consequent variables

$$r^{-}_{i+\frac{1}{2}} = \frac{\theta_i - \theta_{i-1}}{\theta_{i+1} - \theta_i} \quad r^{+}_{i+\frac{1}{2}} = \frac{\theta_{i+2} - \theta_{i+1}}{\theta_{i+1} - \theta_i}.$$

If the limiter is activated the discretization becomes upwind-biased and numerical dissipation is introduced. In the present case a mixture fraction was restricted to lie between 0 and 1, otherwise solution eventually diverged. This was the case both in the TVD-limited and the unlimited case. Fig. 13 shows the mean mixture fraction in the central plane. The TVD-limited scalar does not spread as much as the non-limited scalar. Both schemes underestimate the

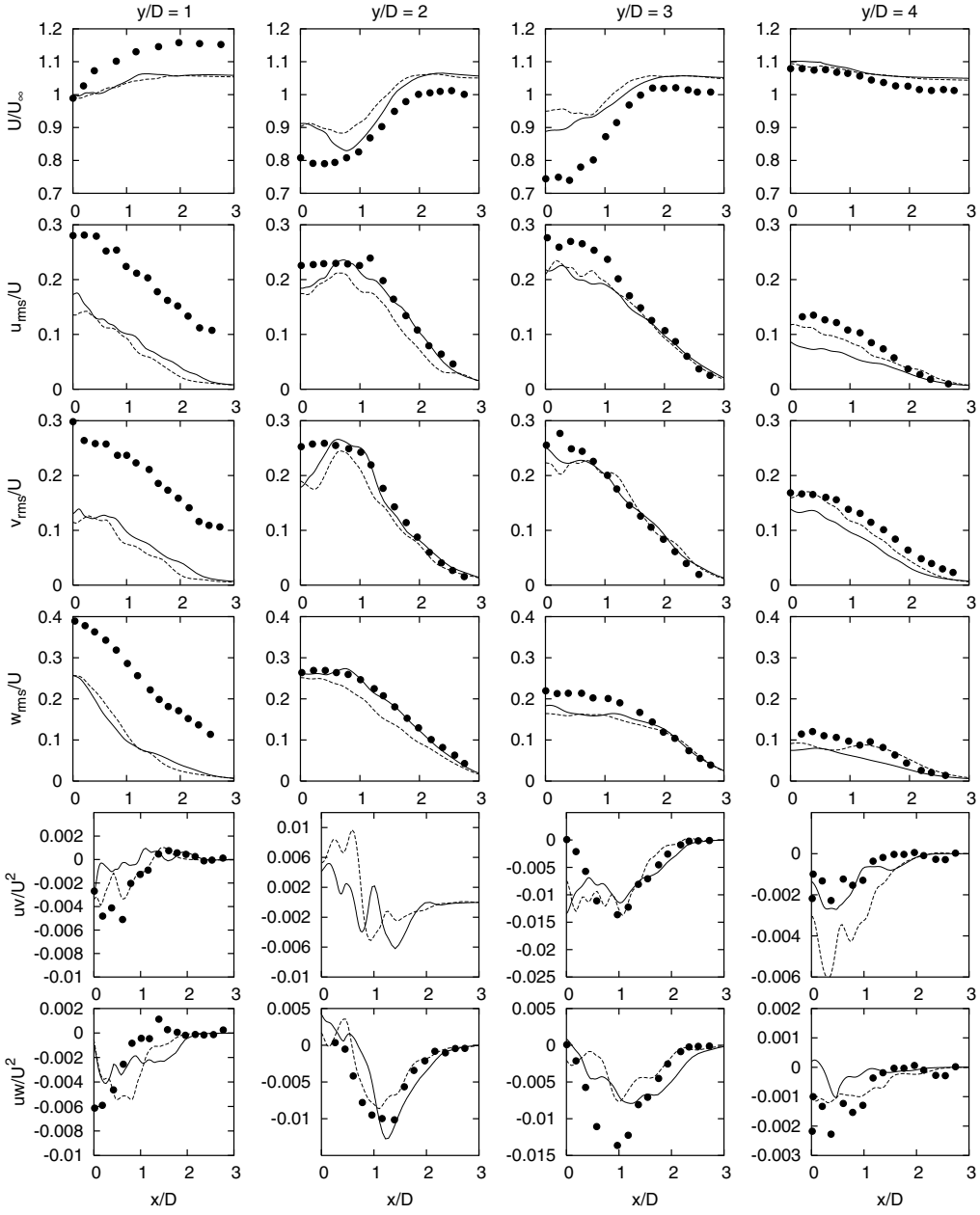

Fig. 12. Mean velocity and Reynolds stress profiles at the position $x/D = 8$ at various distances y/D from the wall and z/D from the central plane: LESUBC (—), LESSBC (---), Crabb et al. (1981) (●).

spreading under the jet. The non-limited scalar fluctuates more than the limited scalar which explains the differences in the spreading. The schemes showed no clear difference in magnitudes for the stream-wise turbulent scalar transport. In other directions the transport terms were not recorded. Only a non-limited scalar discretization was used with LESUBC. The time evolving boundary in the jet pipe affects the scalar spreading even at the far field. The effect is stronger on the scalar field than on the velocity field. The observations above are confirmed by the contour plot (Fig. 14) in the far field plane at $x/D = 8$. The TVD-limited scalar is shown on the right and the non-limited scalar of the LESSBC and the LESUBC in the centre. The measured contours of CDW are plotted with solid lines with the values next to them. Like the experiment, the LESUBC shows separated region for $\theta/\theta_J = 0.22$. Apparently the far field values are not converged completely as these regions are not symmetrically centered.

Fig. 14 shows that in the flow the rich helium concentration does not coincide with the maximum velocity on the right. The flow with higher momentum thus originates from the free-stream fluid accelerated around the jet. The simulated velocity U/U_∞ is flatter on the whole plane, as also seen in Fig. 6. The LES contours are shown with dashed lines whose values lie in the range 0.9–1.04. The smallest values are close to the bottom wall and in the

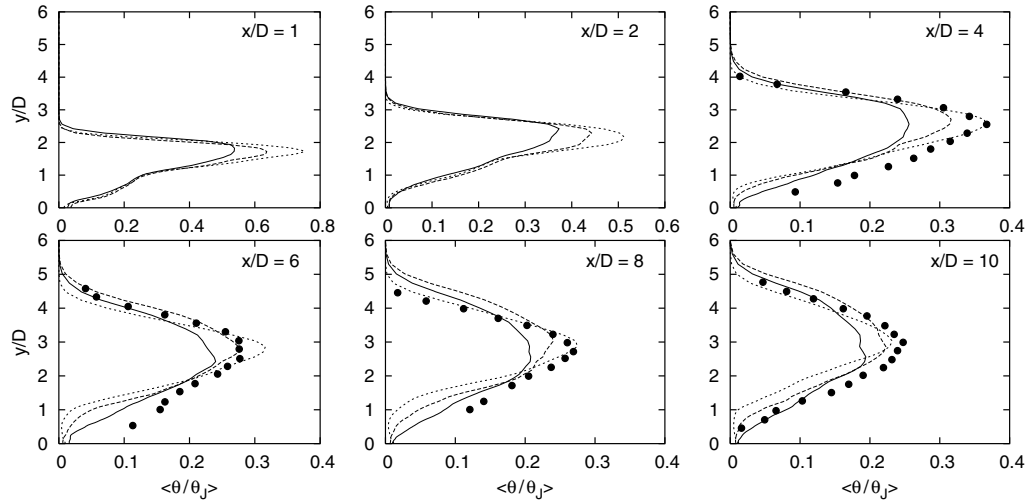

Fig. 13. Mean mixture fraction in the central plane, $z/D = 0$. LESUBC without any limiter (—), LESSBC without any limiter (---), LESSBC with the minmod limiter (···), Crabb et al. (1981) (●).

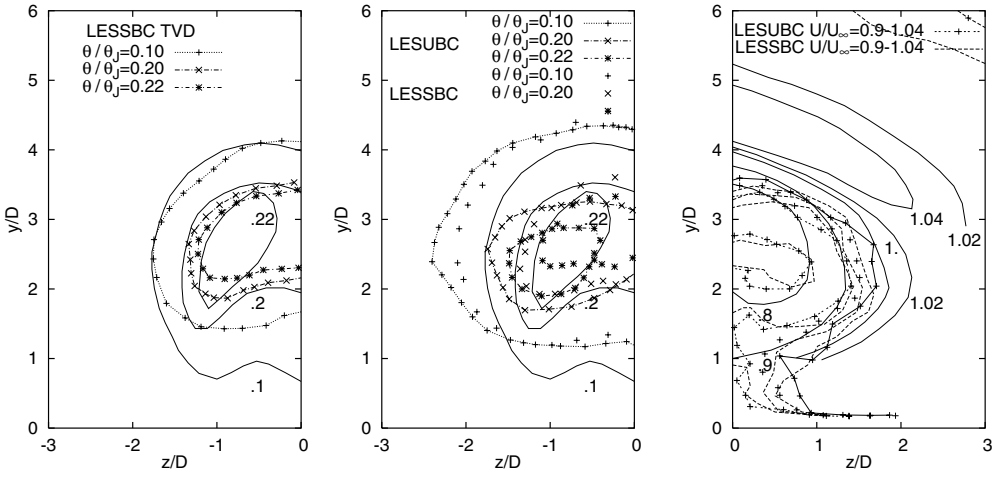

Fig. 14. Contours of the mixture fraction and the mean stream-wise velocity in the plane, $x/D = 8$. The TVD-limited scalar on the left. In the centre the non-limited scalar and on the right the velocity with the LESUBC and LESSB. In all figures the solid line is the data from Crabb et al. (1981).

center plane, a value 1.04 is detected also in the upper corner. The LESSBC and LESUBC velocity contours show no significant differences in this plot.

6. Conclusions

The LES of a turbulent jet in a cross-flow with the present parameters has been performed with the steady-state and the unsteady boundary conditions. On the whole differences between the cases are relatively small in this flow. The LES with the unsteady condition possesses a stronger back-flow in the lee of the jet where the cross-stream-wise velocity profiles along the vertical lines are steeper. In the far field ($x/D \geqslant 8$) the differences are small. The unsteady boundary increased the mixing of the scalar. The scalar was discretized with a TVD scheme in order to reduce the spurious wiggles which consequently reduced also the mixing. In the preliminary computation with a smaller Reynolds number the minmod limiter with the second-order central difference did not completely remove the spurious values.

The resolution near the walls may be too coarse for the present LES in which the flow is resolved to the wall with a no-slip boundary condition. A wall model or a hybrid RANS-LES model might be a good alternative if such a flow is computed with a similar resolution.

The LES reproduced many phenomena present in such a flow, like the shear layer ring vortices and the counter-rotating vortex pair. In general, a reasonable agreement with the measurements was obtained. The LES predicts an intense back-flow near the flat wall where no experimental data is available. It is possible that such a recirculation exists, but in any case the LES predicts it to be too high above the wall and probably too intense.

Acknowledgments

This research project has been funded by the Ministry of Education through Graduate School in CFD and National Technology Agency of Finland TEKES. Also CSC, the Center of Scientific Computation, is acknowledged for providing the IBM cluster.

References

Andreopoulos, J., 1982. Measurements in a jet-pipe flow issuing perpendicularly into a cross stream. Journal of Fluids Engineering 104, 493–499.

Andreopoulos, J., Rodi, W., 1984. Experimental investigations of jets in a crossflow. Journal of Fluid Mechanics 138, 93–127.

Cabot, W., Moin, P., 1993. Large eddy simulation of scalar transport with the dynamic subgrid-scale model. In: Galperin, B., Orszag, S.A. (Eds.), Large Eddy Simulation of Complex Engineering and Geophysical Flows. Cambridge University Press, Cambridge, UK, ISBN 0-521-43009-7, pp. 141–158 (Chapter 7).

Crabb, D., Duráo, D., Whitelaw, J., 1981. A round jet normal to a crossflow. Transactions of the ASME: Journal of Fluids Engineering 103, 568–580.

Hirsch, C., 1990. Computational Methods for Inviscid and Viscous Flows. Numerical Computation of Internal and External Flows, vol. 2. John Wiley & Sons Ltd., Chichester, ISBN 0-471-92351-6.

Keffer, J., Baines, W., 1963. The round turbulent jet in a cross-wind. Journal of Fluid Mechanics 15, 481–497.

Kelso, R., Lim, T., Perry, A., 1996. An experimental study of round jets in cross-flow. Journal of Fluid Mechanics 306, 111–144.

Majander, P., 2000. Developments in large eddy simulation. Report 128. Helsinki University of Technology. ISBN 951-22-4861-1.

Majander, P., Siikonen, T., 2003a. Large eddy simulation of a round jet in a crossflow. Report 142. Helsinki University of Technology. ISBN 951-22-6742-X.

Majander, P., Siikonen, T., 2003b. A parallel multi-block Navier–Stokes solver for large-eddy simulation in complex flows. In: VIII Suomen mekaniikkapäivät, TKK, Espoo, Finland, pp. 395–406.

Smagorinsky, J., 1963. General circulation experiments with the primitive equations. Part I. The basic experiment. Monthly Weather Review 91, 99–152.

Wegner, B., Huai, Y.A.S., 2004. Comparative study of turbulent mixing in jet in cross-flow configurations using les. International Journal of Heat and Fluid Flow 25, 767–775.

Wille, M., 1997. Large eddy simulation of jets in cross flows. Ph.D. thesis. Imperial College of Science, Technology and Medicine, Department of Chemical Engineering, London.

Yuan, L., Street, R., Ferziger, J., 1999. Large-eddy simulations of a round jet in crossflow. Journal of Fluid Mechanics 379, 71–104.